Desalination and Water Treatment
www.deswater.com

doi: 10.1080/19443994.2015.1024743

57 (2016) 6670–6679
March

Taylor & Francis
Taylor & Francis Group

Influence of environmental parameters on the corrosion behavior of 90/10 cupronickel tubes in 3.5% NaCl

Hosni M. Ezuber*, Abdulla Al Shater

Chemical Engineering Department, College of Engineering, University of Bahrain, P.O. Box 32038, Isa Town, Bahrain, Tel. +973 39025954; Fax: +973 17680935; email: halzubair@uob.edu.bh (H.M. Ezuber), Tel. +973 39056021; Fax: +973 17680935; email: aalshater@uob.edu.bh (A. Al Shater)

Received 3 July 2014; Accepted 22 January 2015

ABSTRACT

The paper describes an experimental study concerning the influence of major environmental parameters (temperature, chloride, carbon dioxide, and oxygen) on the corrosion behavior of 90/10 Cu–Ni alloys widely used for heat-transfer tubes. Electrochemical techniques have been used to investigate the corrosion behavior of 90/10 Cu–Ni alloys in aerated 3.5% NaCl solutions, at temperatures of 25, 50, and 80℃ with and without the injection of carbon dioxide. The results have revealed increases in chloride corrosion rates of the 90/10 Cu–Ni alloy with temperature and decreases with CO_2 presence. Tests performed in aerated chloride–CO_2 solutions have shown higher corrosion rates relative to those conducted in deaerated chloride solutions saturated with CO_2 species. The surface morphology of polarized specimens in chloride solutions with and without CO_2 presence has shown a susceptibility to pitting attack. Pit characteristics have been found to be highly influenced by CO_2 presence.

Keywords: 90/10 copper nickel alloys; Chloride ions; CO_2; Corrosion

1. Introduction

Heat exchanger tubings represent the largest procured item in an multistage flash (MSF) plant and more than 70% of the corrosion failures in desalination plants are attributed to heat exchanger tubes [1]. The proper selection of tubing materials is one of the important factors in their efficient and important economic operation of power generation heat exchangers. Many factors are involved in this selection, including cost, corrosion resistance, weldability, and ease of fabrication. As the choice of materials has a great influence on the overall economics of the process, it is important that the correct selection be made [1,2]. Copper–nickel alloys, nickel-base alloys, titanium and stainless steel alloys are the most commonly employed metallic heat exchanger tubing materials in desalination plants. All the materials referred to above may suffer from some sort of corrosion due to improper selection of material, inadequate design, bad operating practice, or poor maintenance [1–3]. Stainless steels and in particular austenitic types (304 and 316) are commonly used due to their excellent resistance to general corrosion and to erosion corrosion even at high seawater velocity. The alloys have good mechanical strength, easy to handle, and fabrication along with good availability of products and moderate cost. The susceptibility of the common austenitic grades (304 and 316) to pitting attack in saline water led to the utilization of highly alloyed grades, most

*Corresponding author.

commonly austenitics 6Mo grades, such as 254 SMO (UNS SS1243) in desalination plant. These alloys exhibit excellent resistance toward pitting corrosion. Higher costs due to more costly alloying elements appear to be the main limitation in using these alloys [4–6]. However, a new generation of duplex grades is entering this industrial field due to a number of reasons. Duplex stainless steels have good resistance to corrosion, especially to stress corrosion cracking, they have twice the strength of austenitic grades, they are less costly due to lower contents of mainly nickel and molybdenum, and they are exceptional engineering materials [5,6]. High chromium containing Ni-base alloys (NI–Cr–Mo) are used as a possible replacement for stainless steels to combat localized corrosion. However, the prohibitive cost of Ni-base alloys has severely restricted their application [7]. Titanium is considered as a superior material for many industrial applications including the manufacture of condenser tubes in MSF plants because of its resistance to corrosion. These materials offer higher scaling and fouling resistance and can help avoid loss of heat exchanger performance over time due to tube plugging. The higher cost, relatively low thermal conductivity, and the current fabrication process make the tubing cost concerning for many applications in which it would fittingly be the material of choice [1,2,7,8].

Copper–nickel alloys and in particular 90–10 and 70–30 cupronickel alloys have found extensive applications in desalination plants as heat exchanger materials due to their high thermal conductivity, remarkable corrosion resistance, and excellent heat-transfer properties. Of these alloys, the 90–10 cupronickel material has become the standard condenser tube materials for desalination plant tubing due to its relatively low cost and remarkable corrosion resistance characteristics allied with outstanding anti-fouling properties [1,2,9]. The good corrosion performance of the 90/10 Cu–Ni alloys has been attributed to the formation of a protective film of Cu(I) oxide, Cu_2O, with nickel and iron compounds as minor constituents. The presence of nickel or iron atoms in the copper compound lattice decreases number of defects and inhibits the formation of deleterious phases thus improving passive film performance [9,10]. Nickel also exhibits the potential for beneficial contribution toward alloy mechanical strength (creep resistance in particular), while the presence of iron enhances resistance to general corrosion and impingement attack in marine environments [11,12]. The onset of beneficial role of iron might be realized at iron content up to 2%. Iron content in excess of 2% leads to sever segregation which is detrimental to the corrosion resistance of the 90–10 cupronickel material [12–15]. Unlike stainless steel and nickel-base alloys, the cupronickel materials are subject to impingement attack in turbulent seawater or brine. They are also known to suffer pitting attack when exposed to marine environments containing dissolved CO_2 [16]. Even in the absence of chloride species, dissolved CO_2 is reported to cause serious vapor-side corrosion problems of cupronickel alloy tubes in the high-temperature stages of MSF desalination units [17–20]. The intensity of the corrosion attack is increased with increasing temperature [19]. The presence of CO_2 in MSF desalination plants is caused mainly by the thermal decomposition of HCO_3^-. CO_2 is usually removed directly by a vent system or even by passing through a decarbonator before further degassing in the deaerators. In case of inefficient ventilation, some CO_2 tends to dissolve and subsequently attack the protective oxide film on condenser tube surfaces [14].

The present study is initiated with the primary objective to experimentally examine the effect of CO_2 presence on the corrosion rate of 90/10 cupronickel alloys commonly used in MSF plants, especially as a heat exchanger tubing material in aerated and deaerated 3.5% NaCl (simulated seawater) as a function of temperature.

2. Experimental details

The chemical composition of the alloy investigated as determined by SEM-EDX is given as follows in (wt.%); Ni: 9.93, Fe: 1.74, Mn: 0.7, S: 0.015, and Cu: balance. The samples were cut from 15 mm diameter pipe. The pipe was cut longitudinally and flattened with a roller. Samples with an insulted electrical connection were mounted in epoxy resin exposing an area of 20 × 20 mm.

The exposed faces of the specimens under investigation were ground down to a 1000-grit SiC surface finish. The specimens were then washed with distilled water and dried. The 3.5% NaCl solution was made with NaCl of analytical grade and distilled water. A pressurized CO_2 cylinder was used for the preparation of saturated CO_2 solutions.

The corrosion process was electrochemically monitored through applying DC potentiodynamic sweeps utilizing an analog ACM potentiostat coupled with a sweep generator. Tests were conducted on a typical three-electrode (500 ml capacity) electrochemical cell comprising a saturated calomel reference electrode, a platinum auxiliary electrode, and the 90–10 cupronickel as the working electrode. A test solution 300 ml in volume was consistently maintained throughout testing in which the three electrodes were directly

immersed. Investigations were carried out with the cells described either open to air or sealed (air tight) depending on whether or not aeration effects were being examined, respectively. For CO_2 injection, a two hour bubbling period was deployed prior to test commencement during which the working electrode was held above test solution level. The injection process was later on continued throughout the testing period, but with the working electrode fully immersed and while maintaining a reduced bubbling rate. The pH of the test solutions was measured at 25℃. In chloride–CO_2 solutions, the pH was found to change during the first five minutes before reaching a final saturation value. The final pH values of the various test solutions are given in Table 1. The test temperature, in the vicinity of 20, 50, or 80℃ was controlled fairly accurately by means of a water bath.

Corrosion measurements were performed consistently following an hour of monitoring the open-circuit potential (E_{ocp}) of the test material. The polarization scans comprised scanning the fresh specimen electrode potential from the E_{OCP} at 1 mVs^{-1} in either the positive (anodic) or negative (cathodic) direction across a potential range of ($E = E_{OCP} \pm 200$ mV). It was from the polarization curves generated the information on Tafel slopes (β_a and β_c) was extracted. The polarization resistance (R_p) was determined by polarizing specimens across a breadth of potential spanning ± 10 mV on either side of E_{OCP}. The instantaneous corrosion current was calculated from the polarization resistance and Tafel slopes using the Stern–Geary equation [21]:

$$i_{corr} = \frac{B}{R_p} = \frac{\beta_a \beta_c}{2.303\, R_p\, (\beta_a + \beta_c)} \quad (1)$$

where R_p = slope of the polarization resistance plot, Ω cm^2, (E–i diagram at $E = E_{OCP} \pm 10$ mV); β_a and β_c = anodic and cathodic Tafel constants, respectively, (V $decade^{-1}$); and i_{corr} = corrosion current density (A cm^{-2}). The penetration rate (in mmpy) was calculated using Faraday's law.

$$\text{CR (mmpy)} = \frac{Z \times i \times t \times 10}{\rho \times n \times F} \quad (2)$$

Table 1
pH of experimental solutions used in this work

	Solution	pH
1	0.6 M NaCl	6.8
2	0.6 M NaCl + CO_2 (sat.) deaerated	3.33
3	0.6 M NaCl + CO_2 (sat.) aerated	3.96

where Z is average atomic weight (≈ 63.06 g mol^{-1}), n is number of electrons (2 electrons), F is Faraday's constant (96,500 A s mol^{-1}), "t" is time (s) (31,536,000 s yr^{-1}), "i" is current density (A cm^{-2}), and "ρ" is density of 90–10 cupronickel material (≈ 8.945 g cm^{-3}).

3. Results and discussion

3.1. Polarization behavior in 3.5% NaCl

Fig. 1 shows typical polarization scans on the 90–10 cupronickel alloy in aerated 3.5% NaCl solutions at 23, 50, and 80℃. The results presented in this figure are thoroughly discussed in earlier work [15]. The main features of this figure may be outlined as:

(1) The open circuit potential, E_{OCP}, is shifted toward more negative values due to temperature rising and the relationship is approximately linear.
(2) All anodic polarization curves (conducted at 25, 50, or 80℃) show three main regions of potential: (i) an apparent Tafel region close to E_{ocp} (typical abrupt increase in current with potential). (ii) with increase in the potential, a small peak of maximum current is attained (Fig. 2). This, however, is followed by current drop to a minimum value followed by gradual increase with increasing potential forming a plateau of almost limited current. The peak maximum, minimum, and limiting current densities show larger values at higher test

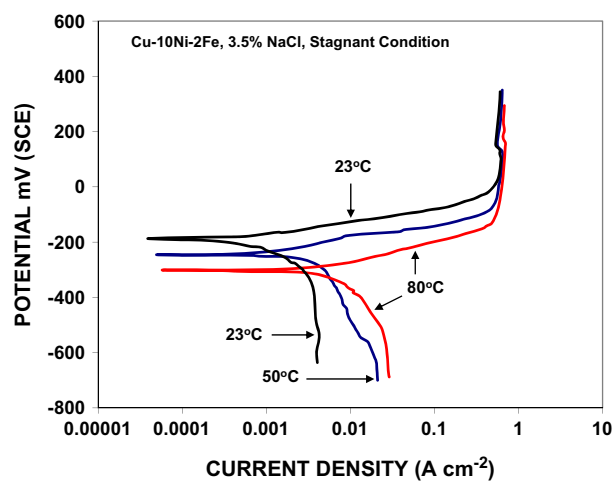

Fig. 1. Effect of test temperature on the potentiodynamic polarization curves of Cu–10Ni–2Fe in aerated 3.5% NaCl solutions.

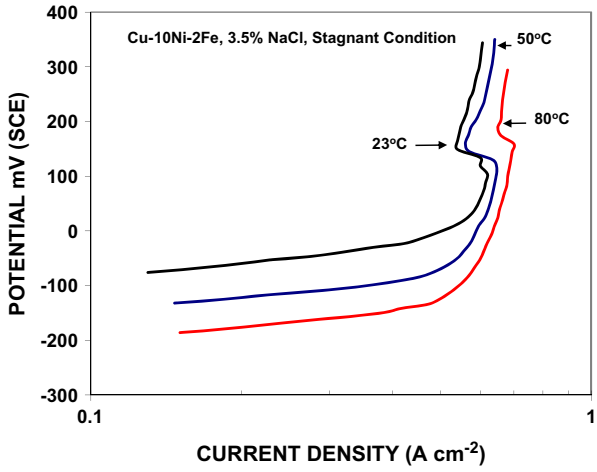

Fig. 2. Effect of test temperature on the anodic polarization curves of Cu–10Ni–2Fe prior to limiting current densities.

temperatures. Fig. 2 also shows that the peak current maximum and minimum appear to diminish with increasing test temperature. (iii) above this limiting region, the current increases due to the formation of divalent copper species [22].

(3) Analysis of anodic curves shows Tafel slopes of approximately 0.059–0.071 V decade^{-1} for the temperature range 25–80℃. The Tafel slope value of 0.059 V decade^{-1} at 25℃ is corresponding well to 2.3 RT/F (R, T, and F are the molar gas constant (8.314 J mol^{-1} K^{-1}), the absolute temperature (K), and Faraday constant, respectively), supporting that Tafel behavior is exhibiting mixed charge transfer and mass transport control kinetics [23].

The corrosion behavior of copper materials at the E_{OCP} is related to the stability of the formed passive layer. When exposed to aerated aqueous solutions, copper undergoes chemical transformations at the surface leading to the formation of oxide films. Auger measurements for copper exposed to chloride solutions, at E_{OCP}, have revealed a dual CuCl/Cu_2O layer at primary stages followed by an eventual growth of a pure Cu_2O thin layer [24]. This has been further supported by other work reporting a dominant presence of Cu_2O as a major compound within surface layers formed on Cu tested in an aerated 0.5 M NaCl solution at E_{OCP}. This formation of the Cu_2O has been attributed partly to the hydrolysis of the $CuCl_2^-$ within the diffusion layer [25]. The crystal structure of the Cu_2O is a quite defective "p" type semiconductor. Ion transport through such a structure is relatively easy because of the wealth of cation vacancies and positive holes present [26]. In general, the protective nature of the film formed on copper materials increases with time and is apparently improved by the presence of nickel and iron within the film [23]. Though the alloying additions present in solid solution with copper do not form oxides distinct from that of the base metal, they do modify the semiconducting properties of the Cu_2O lattice by reducing the cation vacancies [27].

The polarization behavior of 90/10 cupronickel alloys in neutral chloride solutions higher than 0.3 M (0.6 M in the present study) is dominated by the dissolution of copper into a soluble Cu(II)Cl_2^- according to the following processes [23,28]. First, copper is ionized via an electron surface under the influence of Cl^- yielding CuCl adsorbed at the electrode surface.

$$Cu + Cl^- \rightarrow CuCl_{ads} + e^- \quad (3)$$

This CuCl has poor adhesion and transforms into the soluble $CuCl_2^-$

$$CuCl_{ads} + Cl^- \rightarrow CuCl_2^- \quad (4)$$

The resultant soluble ion complex is then hydrolyzed to form a passive Cu_2O layer [25], possibly according to [28];

$$2CuCl_2^- + H_2O \rightarrow Cu_2O + 4Cl^- + 2H^+ \quad (5)$$

In essence, the dissolution process of the cupronickel alloy is controlled by the formation of the CuCl film and the mass transport of $CuCl_2^-$ species from film/solution interface into bulk solution. It follows that the formation of small anodic peaks might be associated with the formation and dissolution of adsorbed CuCl precipitates constituting the film formed at critical current densities [29].

The rate of cathodic reaction is probably underpinned by oxygen reduction kinetics in the neutral solution;

$$O_2 + 2H_2O + 4e^- \rightarrow 4(OH)^- \quad (6)$$

Corrosion rates of the cupronickel alloy in 3.5% NaCl exhibit increasing values as the solution temperature is raised, thereby corresponding well with the negative shift of E_{OCP} (Table 2). This may be attributed to changes in passive film properties with rise in temperature, namely manifested in an increased porosity with temperature, as often suggested, thus resulting in a proliferation of active sites on the alloy surface through which the dissolution process is facilitated.

Table 2
Corrosion behaviors of 90Cu–10Ni alloys in quiescent 3.5% NaCl and/or CO_2 solutions

Temperature	23°C			50°C			80°C		
Solution	NaCl	NaCl–CO_2 (aerated)	NaCl–CO_2 (deaerated)	NaCl	NaCl–CO_2 (sat.)	NaCl–CO_2 (deaerated)	NaCl	NaCl–CO_2 (sat.)	NaCl–CO_2 (deaerated)
E_{OCP} (mV) SCE	−185	−460	−533	−246	−490	−563	−300	−515	−600
CR (*mmpy*)	0.0094	0.0039	0.002	0.0158	0.0071	0.003	0.0557	0.016	0.0077

Despite the decrease in dissolved oxygen concentration, that would otherwise support reaction 4, with the rise in solution temperature, the latter would simultaneously facilitate the diffusion of oxygen and hence the observed induction of heightened corrosion rates [30]. The results presented in Table 2 are in good agreement with the literature [31,32].

3.2. Effect of CO_2 presence

A similar E_{OCP} monitoring procedure was adopted prior to commencement with testing in chloride–CO_2 solutions to that used with plain aerated chloride solutions. Generally, the E_{OCP} shows negative shift with time after initial immersion until a relatively stabilized value of potential is reached. Steady-state potentials at 25, 50, and 80°C were established within 30 min of immersion and their values are given in Table 2. It might be depicted from this table that the presence of dissolved CO_2 in aerated or deaerated 3.5% NaCl solutions has caused a significant effect on E_{OCP}. Essentially, E_{OCP} becomes more negative (active) with CO_2 additions. In particular, E_{OCP} values in the deaerated CO_2 solutions are more active (negative) than those in aerated CO_2 solutions. Moreover, it has been observed that with an increase in test temperature, E_{OCP} is found to attain more active values.

The significant decrease in E_{OCP} as a result of CO_2 presence might be taken to indicate that CO_2 plays an indisputable role in manipulating properties of metal films in chloride environments. Interestingly, the effect of CO_2 on the chloride E_{OCP} is consistent with the results reported for stainless steel alloys [33–35]. The mechanism through which detrimental species are generated comprises a sequence of successive steps. Initially, carbon dioxide gas hydrates in water and changes to carbonic acid, H_2CO_3, which dissociates as below [36]

$$H_2CO_3 = H^+ + HCO_3^- \quad (7)$$

$$HCO_3^- = H^+ + CO_3^{2-} \quad (8)$$

The acidification indicated by Eqs. (7) and (8) is likely to play an important role in modifying the film com-

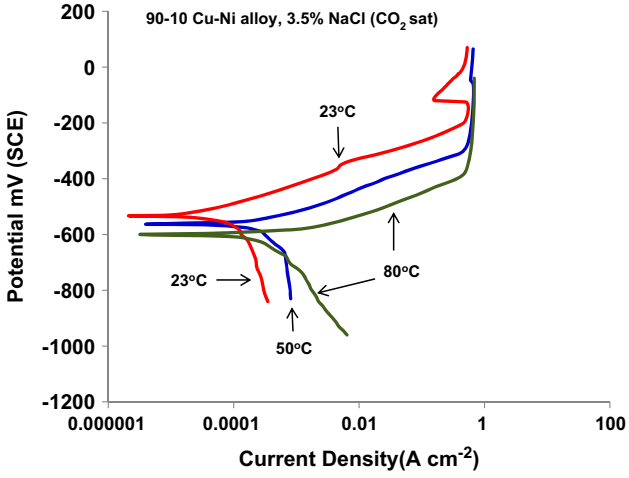

Fig. 3. Effect of temperature on the E-log *i* diagram for 90/10 cupronickel alloy in 3.5% NaCl-deaerated CO_2 (sat.).

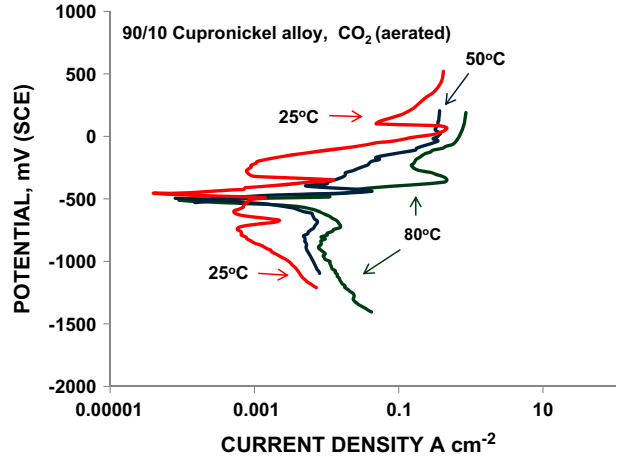

Fig. 4. Effect of temperature on the E-log *i* diagram for 90/10 cupronickel alloy in 3.5% NaCl-aerated CO_2 (sat.).

position on copper nickel alloys resulting in more negative open circuit potentials.

The effect of CO_2 presence on the polarization scans of 90/10 cupronickel alloys in deaerated and aerated 3.5% NaCl is given in Figs. 3 and 4, respectively, and the corrosion parameters are extracted and summarized in Table 2. In deaerated chloride–CO_2 solutions, the curves (Fig. 3) have shown a similar general trend to that exhibited by tests in plain chloride solutions (Fig. 1) except that with the curve pertaining to the 80˚C test solution, no anodic peak was detected. As shown in Fig. 3, the 23˚C anodic curve exhibits a noticeable peak in current density at around −100 mV SCE. The height of the peak diminishes evidently and the peak potential shifts into the positive direction at 50˚C (the peak occurs at about −50 mV SCE). At 80˚C, however, no such peak was recorded as mentioned earlier. Comparing the results at hand to those obtained while testing in plain chloride solutions, anodic peaks in particular (Fig. 2), it might be suggested that CO_2 somehow interferes with the formation and dissolution of adsorbed CuCl precipitates constituting the film formed initially at critical current densities.

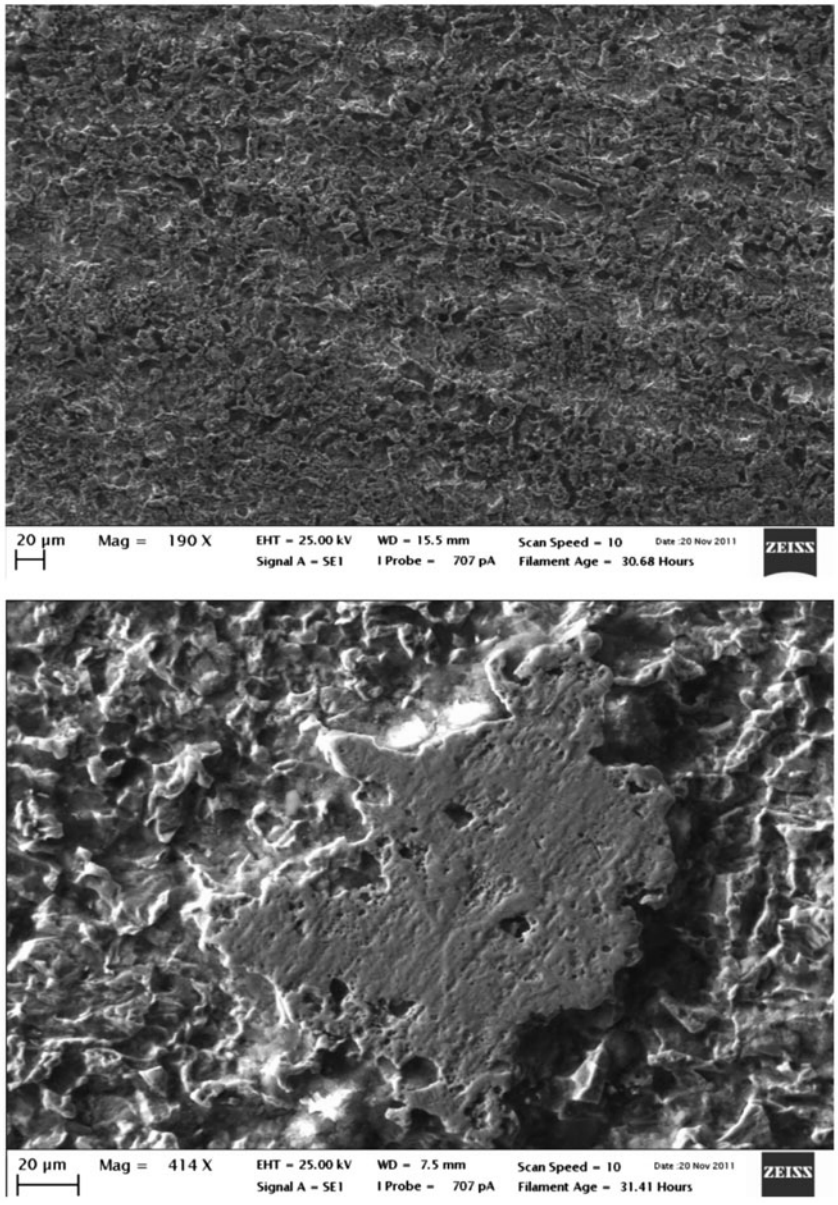

Fig. 5. Surface morphology of 90/10 Cu–Ni alloy after anodic polarization run in 3.5% NaCl at 80˚C.

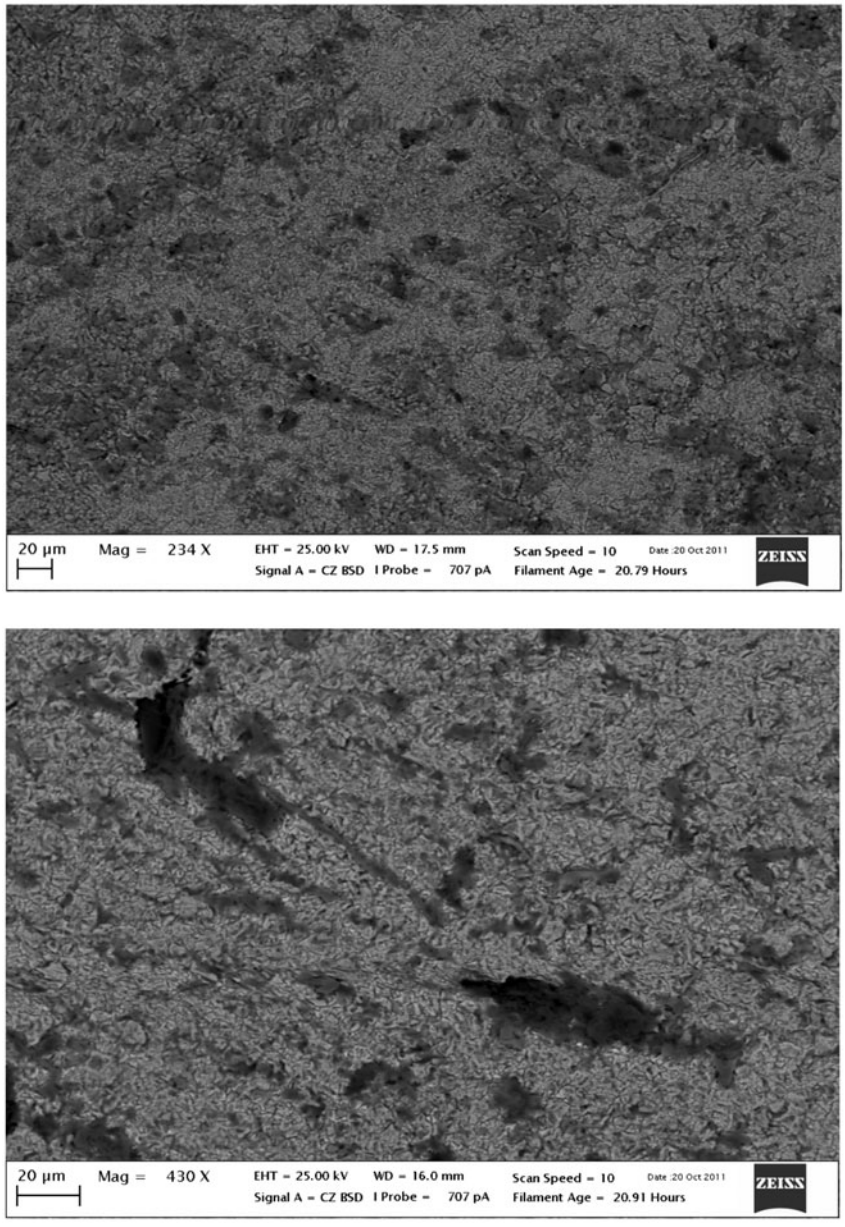

Fig. 6. Surface morphology of 90/10 Cu–Ni alloy after anodic polarization run in aerated 3.5% NaCl–CO_2 solutions at 80˚C.

Ultimately, Fig. 3 shows that the presence of CO_2 results in a noticeable decrease in anodic current, which implies that CO_2 might impede the diffusion of chloride ions toward the alloy substrate as well as the transport of $CuCl_2^-$ to the bulk solution. As a result, the dissolution process is retarded and the corrosion rate is decreased as shown in Table 2.

Polarization curves conducted in aerated chloride–CO_2 solutions are shown in Fig. 4. As shown in this figure, the 90/10 cupronickel alloy starts to corrode at significantly faster rates than in deaerated solutions. The anodic curves of the 90–10 Cu–Ni material exhibited two peaks for 25˚C at around −400 and +50 mV SCE. For 50 and 80˚C, however, only one clear peak was detected for each at around −450 and −350 mV SCE, respectively. The occurrence of the anodic peaks at these potentials may suggest the intervention of dissolved CO_2 and oxygen with the copper chloride salts. Single peaks are also detected in cathodic curves with all test temperatures at around −650 mV SCE. The occurrence of cathodic peaks in aerated chloride containing solutions, particularly at the potential

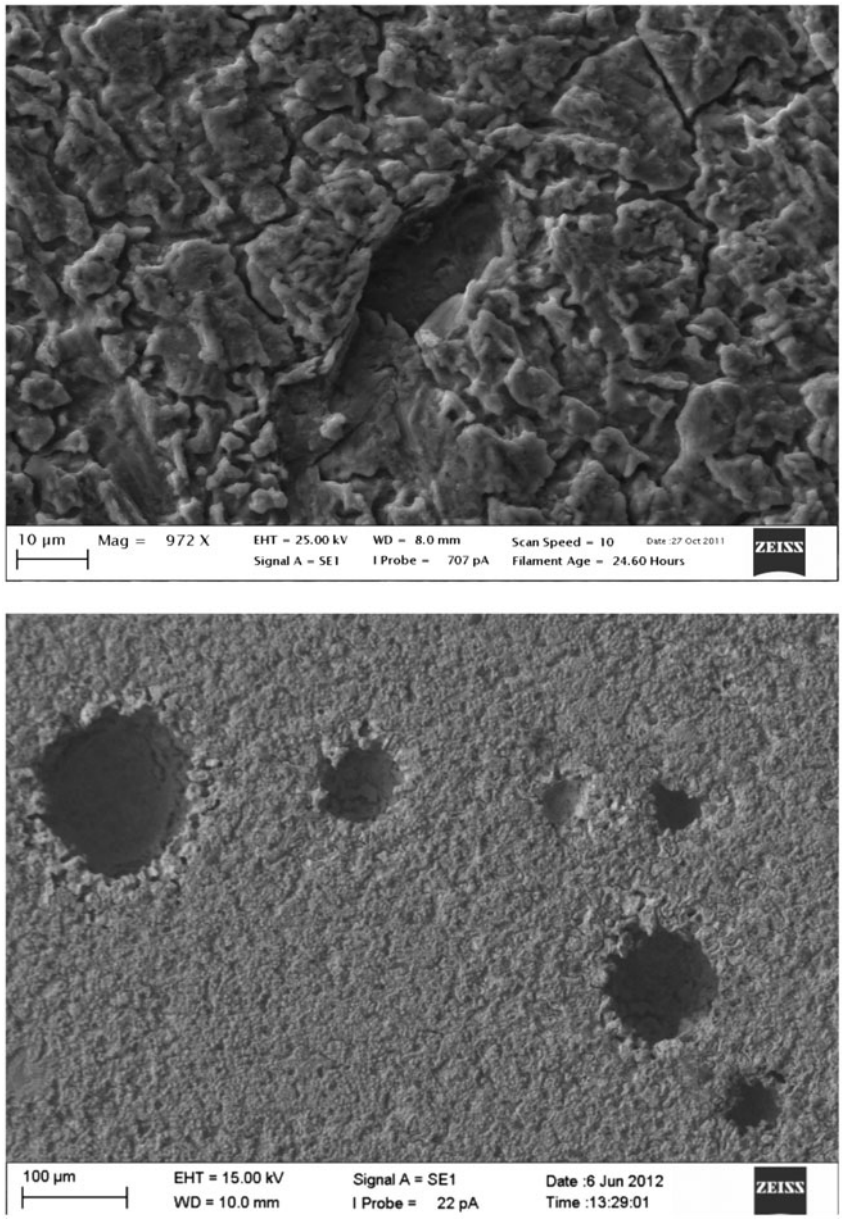

Fig. 7. Surface morphology of 90/10 Cu–Ni alloy after anodic polarization run in deaerated 3.5% NaCl–CO_2 solutions at 80˚C.

specified, has been attributed to the reduction of Cu_2O [28], possibly according to the reaction;

$$Cu_2O + 2H^+ + 2e^- \rightarrow 2Cu + H_2O \quad (9)$$

It has been reported that the anodic dissolution of copper in acidic chloride solutions (pH 1–5) at potentials higher than the dissolution potential of Cu occurs through the mass-transfer controlled step in the Tafel region and the rate of copper oxidation to Cu(I) chloride complexes is independent of pH [37]. The reaction rate is driven by the cathodic reduction of oxygen in an acidic solution

$$O_2 + 4H^+ + 4e \rightarrow 2H_2O \quad (10)$$

The results presented in Table 2 demonstrate a corrosion mitigating effect associated with the presence of CO_2 in aerated and deaerated 3.5% NaCl solutions. This is manifested in a noticeable drop in corrosion rate of 90/10 cupronickel exposed to the various solutions investigated in the order: aerated NaCl > aerated NaCl–CO_2 > deaerated NaCl–CO_2.

3.3. Microstructural investigation

Figs. 5–7 present scanning electron micrographs that were collected as part of a postmortem investigation of the anodically polarized 90/10 cupronickel specimens in aerated/ deaerated chloride solutions with and without dissolved CO_2 species. A pronounced susceptibility to pitting in the identified solutions might be depicted from such micrographs. Overall, pits were characterized by the presence, across the attacked surface, of corrosion product caps. In the absence of CO_2, the surface under examination exhibited severe damage that took the form of highly dense but shallow and rather small pits. The individual pits having hemispherical geometries showed inherent tendencies toward clustering and inevitably coalescing to construct large populations which spread over a large span of the tested area. This phenomenon was found to be in good agreement with Mankowski et al. [38]. In the latter study, Mankowski et al. have shown through X-ray diffraction performed on corrosion products, which constituted similar caps that it was essentially composed of atacamite $CuCl_2.3Cu(OH)_2$. Meanwhile, unlike in plain chloride solutions, the attacked surface in chloride–CO_2 solutions appeared to be covered with a semi-coherent corrosion film with such coherency only interrupted by discretely dispersed/scattered but relatively larger hemispherical pits (with geometry being true even for coalesced pits). This observation was further confirmed by the pitting potential for this test condition being displaced to more negative values. EDAX spectrum analyses of pit bottoms on attacked samples following polarization in chloride–CO_2 solutions have revealed relatively higher carbon contents suggesting an undeniable involvement of CO_2 in underpinning corrosion processes. The mechanism of pit formation in chloride-containing solutions was attributed to successive substitutions of oxygen ions within the initial duplex structure of the passive film (CuO outer layer and Cu_2O inner layer) by chloride ions [38]. This counter-substitution between oxygen and chloride ions then leads to the formation of an insoluble CuCl layer which remains at the alloy surface. Locally, this substitution can proceed further forming $CuCl_2^-$ as demonstrated earlier in Eq. (2).

The sites where the CuCl layer has disappeared mark an onset of preferential metal dissolution with an eventual formation of micro-pits. The dissolution occurs according to the reaction

$$4Cu + 2Cl^- + 6H_2O \rightarrow CuCl_2 3Cu(OH)_2 + 6H^+ + 8e^- \quad (11)$$

The reduced aggressiveness in CO_2 solutions in comparison with plain chloride solutions may be related to the incorporation of carbonates in corrosion products of the former [36]. The scarce of oxygen in deaerated CO_2 solutions is also playing a major role in lowering the corrosion rate.

4. Conclusions

The electrochemical behavior of 90/10 cupronickel alloys in chloride–CO_2 solutions is complex and depends largely on the extent of CO_2 presence, aeration, and test temperature.

The corrosion rate of the 90/10 cupronickel alloy in 3.5% NaCl is increased with temperature, and the severity of which might be mitigated through CO_2 presence.

The corrosion rate of the 90/10 cupronickel alloy in aerated chloride–CO_2 solutions has shown higher corrosion rate than those in deaerated chloride solutions saturated with CO_2 species.

The corrosion potential of the 90/10 cupronickel alloy in 3.5% NaCl is shifted to more negative values with CO_2 presence. The shift is more pronounced in the case of deaerated CO_2 solutions.

Scanning electron micrographs of anodically polarized 90/10 cupronickel specimens in chloride solutions with and without dissolved CO_2 species revealed susceptibility to pitting in these solutions. Pits are characterized by the presence, over the attacked surface, of corrosion product caps. In the absence of CO_2, the attacked surface exhibited severe damage manifested in dense clusters of shallow/small pits. The pits assume hemispherical geometries when discretely present but predominantly exist as coalesced pit clusters. Unlike in plain chloride solutions, the attacked surface in chloride–CO_2 solutions appeared to be covered with corrosion films occasionally interrupted by scattered, however, relatively larger hemispherical pits.

Acknowledgment

The authors would like to thank Hanan Abbas for her role in sample characterization utilizing SEM.

References

[1] A.U. Malik, P.C. Mayan Kutty, I.A. Andijani, A.A. Al-Fozan, Materials performance and failure evaluation in SWCC MSF plants, Desalination 93 (1993) 445–460.
[2] T. Hodgkiess, Current status of materials selection for MSF distillation plants, Desalination 93 (1993) 445–460.

[3] A.U. Malik, S.A. Al-Fozan, F. Al-Muaili, Corrosion of heat exchanger in thermal desalination plants and current trends in material selection, Desalin. Water Treat. (2014), doi: 10.1080/19443994.2014.940642.
[4] J. Olsson, Stainless steels for desalination plants, Desalination 183 (2005) 217–225.
[5] J.W. Oldfield, B. Todd, Duplex—A new generation of stainless steels for desalination plants, Desalination 205 (2007) 104–113.
[6] H.M. Ezuber, A. El-Houd, F. El-Shawesh, Effects of sigma phase precipitation on seawater pitting of duplex stainless steel, Desalination 207 (2007) 268–275.
[7] A. Malik, I. Andijani, M. Mobin, S. Al-Fozan, F. Al-Muaili, M. Al-Hajiri, An overview of the localized corrosion problems in seawater desalination plants—Some recent case studies, Desalin. Water Treat. 20 (2010) 22–34.
[8] C. Sommariva, R. Borsani, P. Peluffo, A. Mollica, C. Wrubl, Titanium exchanger tubes for MSF desalination plant. A study on the aspects relevant to the adaption of this material, Desalination 97 (1994) 53–65.
[9] A.M. El Din, Copper alloys for desalination plants, Desalination 93 (1993) 499–516.
[10] S.J. Yuan, S.O. Pehkonen, Surface characterization and corrosion behavior of 70/30 Cu-Ni alloy in pristine and sulfide-containing simulated seawater, Corros. Sci. 49 (2007) 1276–1304.
[11] R.F. North, M.J. Pryor, The influence of corrosion product structure on the corrosion rate of Cu-Ni alloys, Corros. Sci. 10 (1970) 297–311.
[12] A. Barbucci, G. Farne, P. Matteazzi, R. Riccieri, G. Cerisola, Corrosion behaviour of nanocrystalline Cu90Ni10 alloy in neutral solution containing chlorides, Corros. Sci. 41 (1998) 463–475.
[13] T. Burleigh, D. Waldeck, Effect of alloying on the resistance of Cu-10% Ni alloys to seawater impingement, Corrosion 55 (1999) 800–804.
[14] O. Elragei, F. Elshawesh, Corrosion failure 90/10 cupronickel tubes in a desalination plant, Desalin. Water Treat. 21 (2010) 17–22.
[15] H. Zubeir, The role of iron content on the corrosion behavior of 90Cu-10Ni alloys in 3.5% NaCl solutions, Anti-Corros. Methods Mater. 59 (2012) 159–202.
[16] K. Abouswa, F. Elshawesh, O. Elragei, A. Elhood, Corrosion investigation of Cu-Ni tube desalination plant, Desalination 205 (2007) 140–146.
[17] N. Asrar, A. Malik, S. Ahmad, A. Al-Sheikh, F. Al-Ghamdi, M. Al-Thobiety, Early failure of cupronickel condenser tubes in thermal desalination plant, Desalination 116 (1998) 135–143.
[18] D. Mantzavinos, T. Hodgkiess, S.L. Lai, Corrosion of condenser tube materials in distilled water, Desalination 138 (2001) 365–370.
[19] K.Z. Al-Subaie, T. Hodgkiess, Corrosion of copper-nickel alloys in simulated vapourside environments, Desalination 158 (2003) 43–50.
[20] M.A. Al-Thubaiti, T. Hodgkiess, S.Y. Ho, Environmental influences on the vapourside corrosion of copper-nickel alloys, Desalination 183 (2005) 195–202.
[21] F. Mansfeld, Polarization resistance measurements-experimental procedure and evaluation of test data, in: R. Baboian (Ed.), Electrochemical Techniques for Corrosion, NACE, Houston, TX, 1977, pp. 18–26.
[22] W. Chen, S. Hong, H.B. Li, H.Q. Luo, M. Li, N.B. Li, Protection of copper corrosion in 0.5 M NaCl solution by modification of 5-mercapto-3-phenyl-1,3,4-thiadiazole-2-thione potassium self-assembled monolayer, Corros. Sci. 61 (2012) 53–62.
[23] G. Kear, B.D. Barker, K. Stokes, F.C. Walsh, Electrochemical corrosion behaviour of 90–10 Cu–Ni alloy in chloride-based electrolytes, J. Appl. Electrochem. 34 (2004) 659–669.
[24] G. Bech-Nielsen, M. Jaskula, I. Chorkendorff, J. Larsen, The initial behaviour of freshly etched copper in moderately acid, aerated chloride solutions, Electrochim. Acta 47 (2002) 4279–4290.
[25] E.M. Sutter, B. Millet, C. Fiaud, D. Lincot, Some new photoelectrochemical insights in the corrosion-passivation processes of copper in aqueous chloride solution under-open circuit conditions, J. Electroanal. Chem. 386 (1995) 101–109.
[26] Y.N. Zhang, J.L. Zi, M.S. Zheng, J.W. Zhu, Corrosion behavior of copper with minor alloying addition in chloride solution, J. Alloys Compd. 462 (2008) 240–243.
[27] R.J. Blundy, M.J. Pryor, The potential dependence of reaction product composition on copper-nickel alloys, Corros. Sci. 12 (1972) 65–75.
[28] J.P. Ferreira, J.A. Rodrigues, I.T.E. da Fonseca, Copper corrosion in buffered and non-buffered synthetic seawater: A comparative study, J. Solid State Electrochem. 8 (2004) 260–271.
[29] D. Tromans, J.C. Silva, Behavior of copper in acidic sulfate solution: Comparison with acidic chloride, Corrosion 53 (1997) 171–178.
[30] Y. Wang, A. Beccaria, G. Poggi, The effect of temperature on the corrosion behaviour of a 70/30 Cu-Ni commercial alloy in seawater, Corros. Sci. 36 (1994) 1277–1288.
[31] K. Habib, Electrochemical behavior of copper-nickel alloys in sulphide polluted seawater at moderate temperatures, Desalination 89 (1992) 41–46.
[32] H. Ezuber, Effect of temperature and thiosulphate on the corrosion behaviour of 90–10 copper-nickel alloys in seawater, Anti-Corros. Methods Mater. 56 (2009) 168–172.
[33] N. Anselmo, J.E. May, N.A. Mariano, P.A.P. Nascente, S.K. Kuri, Corrosion behavior of supermartensitic stainless steel in aerated and CO_2-saturated synthetic seawater, Mater. Sci. Eng. A 428 (2006) 73–79.
[34] H. Ezuber, Metallurgical and environmental factors affecting the pitting behavior of UNS S 32205 Duplex stainless steel in chloride solutions, Mater. Corros. 63 (2010) 111–118.
[35] H. Ezuber, Influence of temperature on the pitting corrosion behavior of AISI 316L in chloride–CO_2 (sat.) solutions, Mater. Des. 59 (2014) 339–343.
[36] M. Nordsveen, S. Nešić, R. Nyborgand, A. Stangeland, A mechanistic model for carbon dioxide corrosion of mild steel in the presence of protective iron carbonate films—Part 1: Theory and verification, Corrosion 59 (2003) 443–456.
[37] C.T. Kwok, P.K. Wong, H.C. Man, F.T. Cheng, Effect of pH on corrosion behavior of CuCrZr in solution without and with NaCl, J. Nucl. Mater. 394 (2009) 52–62.
[38] G. Mankowski, J.P. Duthil, A. Giusti, The pit morphology on copper in chloride- and sulphate-containing solutions, Corros. Sci. 39 (1997) 27–42.